HIGHLY EFFECTIVE SIMULATION MODELS IN ANALYZING AERODYNAMICS OF AIRFOILS AT LOW REYNOLDS NUMBER

The Hung Tran[1,*], Ngoc The Nguyen[2], Van Duy Pham[3], Dinh Anh Le[2]

[1]*Faculty of Aerospace Engineering, Le Quy Don Technical University*

[2]*School of Aerospace Engineering, VNU University of Engineering and Technology*

[3]*School of Mechanical Engineering, Hanoi University of Science and Technology*

Abstract

Recently, much work has been conducted for airfoils at low Reynolds and high velocity for further improving design airplanes those can fly on Mars and on stratosphere of the Earth. In this study, the aerodynamic characteristics of a typical airfoil shape named Ishii are studied by numerical approach for understanding the aerodynamic forces and flow fields at different angle of attack and Mach number. To reduce the numerical time, the Reynolds averaged Navier-Stokes equations are used for the simulation. The numerical results are compared with previous experimental data at the same flow conditions. This study found that the turbulent model should be changed from k-ω SST for angles of attack below 8° to k-ε model for higher angles of attack to obtain the accurate results. The maximum difference between simulation and experimental results is less than 9%. To extend the results, the aerodynamic characteristics were investigated for angles of attack from 0° to 20° and the Mach number between 0.2 and 0.8. The effect of serration at the leading edge on aerodynamic characteristics was also investigated. The results of the current study show that the angle of attack with maximum lift coefficient is around 8° at M = 0.2 and it increases for increasing Mach number. At high angle of attack, the lift decreases but large stall does not occur. The reason is from the generation of a separation bubble at leading edge of airfoil, which shows different characteristics from normal airfoil model. The serration at leading edge increases lift and aerodynamic performance for angles of attack above 8°. The results of the proper orthogonal decomposition indicates that the unsymmetric flow with a large wake structure is the most dominant flow at high angles of attack. The flow pattern of those modes, velocity and pressure distributions around the model are discussed.

Keywords: *Ishii airfoil; computational fluid dynamics; Mars airplane; Mach number; angle of attack.*

1. Introduction

Exploring other planets and designing airplanes have been an interesting topic for mechanical researchers. In recent decades, much work has been conducted on studying airplanes flying on Mars to understand the aerodynamic behavior and increase the aerodynamic performance. In comparison to the atmosphere of the Earth, the air around the

[*] Corresponding author, email: tranthehung_k24@lqdtu.edu.vn

DOI: 10.56651/lqdtu.jst.v20.n02.934

atmosphere of Mars is mainly carbon dioxide with much lower air density and low pressure. The air conditions on Mars lead to change in designing airfoils and airplanes to provide sufficient lift and aerodynamic performance. Generally, the airplane is required to fly at high Mach number and very low Reynolds number conditions [1]. At those conditions, the airfoil for airplanes on Mars is often thinner than that on Earth. Although a helicopter was designed and successful to fly on Mars, many problems and questions regarding to fluid mechanics and aerodynamics still exist [2].

In the review of airplanes in literature, it shows that the aerodynamic behaviors and number of airplane at Mach number between 0.2 and 0.8 with Reynolds number in ranges of 10^4-10^5 are limited. This flow condition is similar to the airplanes that fly on Mars. To understand the flow behavior, much work was conducted by Anyoji *et al.* [3] at Tohoku University by both simulation and experimental methods. At low Reynolds number conditions, a separation bubble was observed in the upper surface of the airfoil for moderate angles of attack. The existence of the separation bubble changes the pressure distribution and aerodynamic force. In fact, a linear of the lift by angle of attack is disturbed at very low angles of attack. Caros *et al.* has focused on numerical simulation algorithms in their research, optimizing the aerodynamic parameters of triangular airfoil wings operating in Martian conditions [4], [5]. It was also shown that the Mars atmosphere is similar to the atmosphere of the Earth at an altitude of around 30 km, where long-range endurance airplane works [6]. Consequently, the researches on these flow conditions also help to improve the aerodynamic performance of airplanes at stratosphere. Those airplanes can work as satellites for transferring signals and they have been focused by many companies, recently. For understanding detailed characteristics of low Reynolds number airfoils, the Ishii airfoil has been developed to reduce the separation flow and increase aerodynamic characteristics [3]. Although many studies have been conducted for that airfoil, high scheme simulation models, such as large eddy simulation, and direct numerical simulation, were applied. The use of those models leads to high numerical time, which is not suitable for the initial design process.

For increasing the aerodynamic performance of low Reynolds number airfoils at high angle of attack, serration at the leading edge is often used. This technique mimics animal wings, which also fly at low Reynolds numbers. Earlier research on sawtooth wing shapes (SLEs) has primarily focused on flat plates featuring serrations along the leading edge of the wing [7]. Findings suggest that the aerodynamic characteristics of serrated-edge flat plates are almost the same as those of standard flat plates, with enhancements in stall angle performance, as shown by Smith and Klettner, who used large eddy simulations for the airfoil flow [8]. The working principle of the serration is

due to the fact that it reduces the velocity fluctuation upstream of the trailing edge and the correlation of the large-scale vortices. This structure can be found on the fins of humpback whales, which sufficiently delays the stall at high angles of attack and helps the animals swim smoothly [9]. Other studies have also investigated the application of serrated trailing edges to reduce noise levels [10]-[12].

From above review, it shows that previous studies used complicated experiments or high numerical schemes for the simulation of the flow around low-Reynolds airfoils. Since the mesh volume is sufficiently high, which was often above 30 million cells, this technique is not suitable for fast prediction of the aerodynamic characteristics during the initial design process. Additionally, it is also a big problem for small laboratories where the supercomputer system is limited. Consequently, low-cost, highly effective techniques are required for the simulation. Regarding a typical airfoil at a low Reynolds number, such as the Ishii airfoil, previous studies were limited to a typical Mach number and for the angle of attack below 15°. The effect of serration on aerodynamics and the stall behavior of the airfoil is not clear and should be further classified.

In this study, the aerodynamic characteristics of the Ishii airfoil in the atmosphere of Mars are studied by computational fluid dynamics (CFD). Different numerical schemes, which are based on the Reynolds averaged Navier-Stokes equation, are tested and adjusted to find the most accurate models for the simulation. The numerical results are validated with experimental data by Anyoji *et al.* [3] at the Mach number of 0.2. It was shown that the k-ω turbulent model is the most accurate model at angles of attack below 8°, while the k-ε model is required for the higher angles. Then, the numerical schemes are applied to study the effect of angle of attack, Mach number, and serration on the aerodynamic force and flow behavior is analyzed.

2. Computational method

2.1. Model geometry and numerical domain

The profile of the Ishii airfoil is illustrated in Fig. 1a, showing a maximum wing thickness ratio of 7.1% at x/c = 0.25 and a peak camber of 2.3% at x/c = 0.62. Here, c represents the chord line of the wing (c = 50 mm). In comparison to the NACA airfoil, the maximum thickness of the Ishii airfoil is much lower, which helps to increase the aerodynamic performance at a high Mach number. This study used simulation method to obtain the full parameters of the flow. Additionally, the experimental results of previous study are used for the validation. The numerical domain is shown in Fig. 1b. Here, the numerical domain contains a circular arc with a radius of r = 16c, a trailing length of 17c, and a width of 2c. The length of the numerical domain is sufficiently

long, which allows to capture of the wake flow at high angle of attack. In this computational domain, the inflow region is positioned in the circular intake area in front of the wing and extends above and below it, with the outflow pressure set to free flow. Both side boundaries of the domain are set as symmetric surfaces, while the wing surface of the airfoil is defined using a wall function.

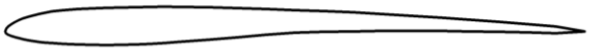

a) Ishii airfoil

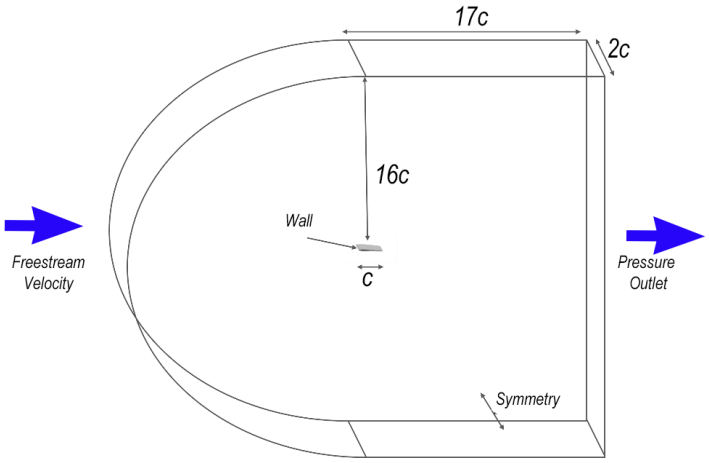

b) Numerical domain

Fig. 1. Airfoil model and numerical domain.

2.2. Mesh generation and numerical method

A structured mesh is applied around the airfoil profile and within the computational domain, with images captured from multiple angles, as illustrated in Fig. 2. Here, Fig. 2a shows the mesh in the whole numerical domain in the symmetric plane while other sub-figures show the zoom-in mesh around the airfoil. The first grid layer adjacent to the wing boundary has a thickness of approximately $4 \cdot 10^{-5}$ m, corresponding to $y^+ \approx 1$, which is suitable for ensuring high accuracy in calculations. The number of layers inside the boundary layer is 40 with a growth rate of 1.15. The distance from the wing region to the boundary layer is sufficiently large to minimize numerical simulation interference from the boundary area. Additionally, the boundary area has a curved shape at the wing's leading edge, which assists in adjusting wind direction and enables analysis across various angles of attack. Before conducting the simulation, mesh sensitivity with mesh cells between 0.4 and 2.0 was tested. Finally, the total cell of around 1.4 million is selected for the simulation. The grid convergence index (GCI) is used to evaluate the

error of the simulation, as it was often used in previous studies [13], [14]. It showed that the GCI of the lift is less than 5%, which guarantees the accuracy of the mesh generation method for the simulation. Note that the mesh volume is much smaller than that of the previous study by Anyoji *et al.* [3] who applied the large eddy simulation. The total number of mesh cells in large eddy simulation is often above 30 million, which requires supercomputers for the simulation. In this study, Reynolds averaged Navier-Stokes (RANS) equations are used for the simulation. In this method, an averaged filter is applied for the Navier-Stokes equations, which include the continuity, moment and energy equations. When the filter is applied, Reynolds shear stress components occur and they are simulated by different turbulent models [15]. Since an averaged filter is applied, only averaged results can be simulated from the simulation. Although the accuracy of RANS is limited, the application of additional equations and hypotheses allows to reduce the numerical time. Additionally, selecting the properly turbulent model and its coefficient can improve the numerical results.

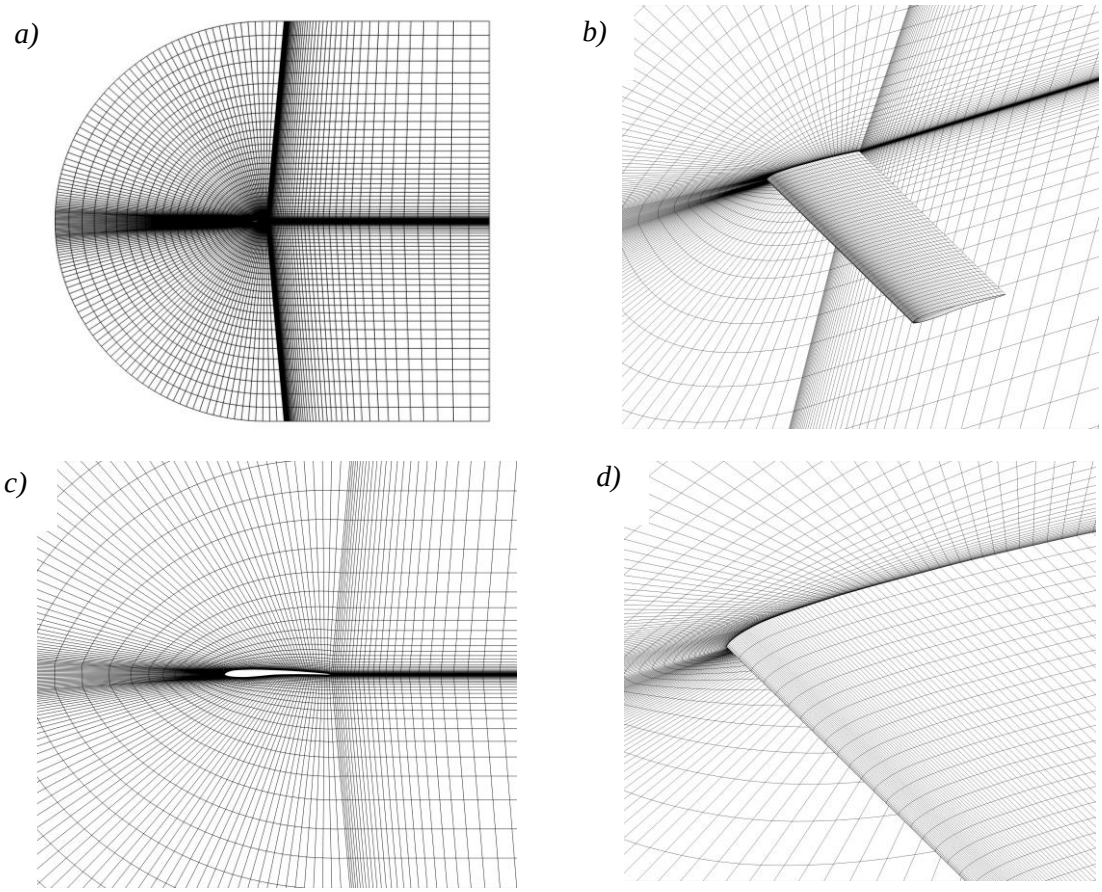

Fig. 2. Mesh around the model.

To simulate the Reynolds shear stresses, the Shear Stress Transfer (SST) *k-ω* computational model is mainly employed for calculations within this domain. The model shows the advantage of quick computation and is particularly effective at addressing flow separation issues around the boundary layer. The transport and turbulent kinetic energy equations are defined by the following expressions [15]:

$$\frac{\partial(\rho k)}{\partial t}+\frac{\partial(\rho u_j k)}{\partial_{x_j}}=P+\beta^*\rho\omega k+\frac{\partial}{\partial_{x_j}}\left[\left(\mu+\sigma_k\mu_t\right)\frac{\partial k}{\partial_{x_j}}\right] \tag{1}$$

$$\frac{\partial\left(\rho\omega\right)}{\partial t}+\frac{\partial\left(\rho u_j\omega\right)}{\partial x_j}=\frac{\gamma}{\nu_t}P-\beta\rho\omega^2+\frac{\partial}{\partial x_j}\left[\left(\mu+\sigma_k\mu_t\right)\frac{\partial\omega}{\partial x_j}\right]+2\left(1-F_1\right)\frac{\rho\sigma_{\omega_2}}{\omega}\frac{\partial k}{\partial x_j}\frac{\partial\omega}{\partial x_j} \tag{2}$$

$$\nu_t=\frac{a_1 k}{\max(a_1\omega;\Omega F_2)} \tag{3}$$

where

$$F_2=\tanh\left[\left[\max\left(\frac{2\sqrt{k}}{\beta\omega y},\frac{500\nu}{y^2\omega}\right)\right]^2\right]$$

$$P_k=\min\left(\tau_{ij}\frac{\partial U_i}{\partial x_j},10\beta k\omega\right)\quad F_1=\tanh\left\{\left\{\min\left[\max\left(\frac{\sqrt{k}}{\beta\omega y},\frac{500\nu}{y^2\omega}\right),\frac{4\sigma_{\omega 2}k}{CD_{k\omega}y^2}\right]\right\}^4\right\} \tag{4}$$

$$CD_{k\omega}=\max\left(2\rho\sigma_{\omega_2}\frac{1}{\omega}\frac{\partial k}{\partial x_i}\frac{\partial\omega}{\partial x_i},10^{-10}\right)$$

$$\phi=\phi_1F_1+\phi_2\left(1-F_1\right)$$

Additionally, ρ is air density, k is turbulent kinetic energy, ω is specific dissipation rate, u_j is velocity component j, P is pressure, v_t is kinematic viscosity, μ is turbulent dynamic viscosity, Ω is an invariant measure of the strain rate, and τ_{ij} is Reynolds stress components. The other constant parameters in the above equations are determined as below:

$$\alpha_1=\frac{5}{9},\ \alpha_2=0.44,\ \beta_1=\frac{3}{40},\ \beta_2=0.0828,\beta^*=0.09,\ \sigma_{k1}=0.85,\ \sigma_{k2}=1,\sigma_{\omega 1}=0.5,$$

and $\sigma_{\omega 2}=0.856$.

The above constant parameters were selected default as recommended by Menter [15]. Note that the SST *k-ω* model shows a high potential for surface flow at

low angles of attack. However, during our calculation, this model shows poor results of lift coefficient for high angle of attack. This is because the SST k-ω model is over prediction of the surface flow and thereby the wake structure is not captured correctly when high separation flow occurs. By different attempts, the k-ε turbulent model with non-equilibrium wall functions is selected for angles of attack above 8°. Regarding to the k-ε turbulent model, two additional equations for k and are ε also used. Those expressions can be received from the above equations with the assumption of $F_2 = 0$. The results of the current study are exported and analyzed using Tecplot and Matlab programs. The flow condition is set the same as in the Mars atmosphere with an air density of $\rho = 0.01841$ at initial conditions. The air is considered a compressible condition. The temperature effects are disregarded. The Mach number, which is determined by the ratio of the velocity of the model to the velocity of the air, is changed from 0.2 to 0.8. Those Mach numbers are typical for airplanes flying on Mars at subsonic conditions. Consequently, the results are validated for other Mach number from 0.2 to 0.8. At $M = 0.2$, the Reynolds number, which is based on the chord length of the wing is set at 23000, with the same flow conditions in previous studies by Anyoji *et al.* [3] for validations. The coupled algorithm is applied to determine velocity and pressure results. A second order in the derivative of velocity and pressure is used. Note that the environment in the simulation may not be exactly the same as that in Mars. However, the results of the current study can be used as a reference for airplanes flying on Mars and the stratosphere. Additionally, in comparison to previous studies, the numerical time of the RANS simulation takes around two hours for each case, which is much smaller than other high-numerical scheme methods.

3. Results and discussions

3.1. Aerodynamic lift at different angles of attack

Figure 4 presents lift coefficient at different angle of attack. Previous results by Anyoji *et al.* [3] are also drawn. For $\alpha > 8°$, the turbulent model is shifted to k-ε to capture the correct lift coefficient. As can be seen, the lift of the current study is highly consistent with previous observations by Anyoji *et al.* The difference occurs only for angles of attack of 12°, where the lift coefficient of the current study is lower than that by Anyoji *et al.* with a maximum difference of 9%. The difference can be explained by the difference in the air condition between the experiment and numerical simulation.

In detail, the flow in the simulation is much smoother than that of the experiments. As a result, separation flow with complex can occur earlier in simulation and the lift is smaller. Additionally, the flow may highly unsteady at high angles of attack (α > 10°), where the stall occurs and it affects the simulation as well as experimental results. Note that the numerical scheme and the method for the calculation of forces are different between the two methods. Previously, Anyoji *et al.* used the large eddy simulation, which consumes a large numerical time in supercomputers. Furthermore, the support system for the model can affect the results. Since this technique is not suitable for initial design process, we used the RANS simulation method. It should be noted that the current simulation cannot provide the unsteady flow and the boundary layer was assumed as a knowing function. However, a similar trend of the lift was obtained with a maximum error less than 9%. In terms of the pressure distribution, which was not shown here, a similar tendency was also observed for the simulation in comparison to experimental data. It is indicated that the current simulation method can provide sufficiently accurate averaged results and can be extended for further discussion. Interestingly, both results present that the stall with a high decreasing lift may not generate at the airfoil at low Reynolds number.

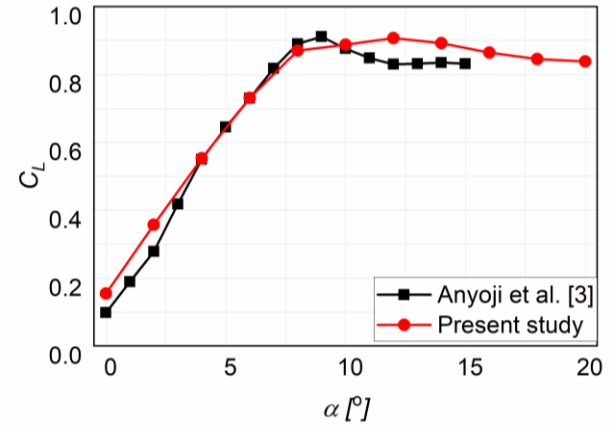

Fig. 4. Lift of the model by angle of attack.

3.2. Velocity and pressure distribution

For the details of the flow, Fig. 5 presents the pressure distribution around the airfoil in the symmetric plane y = 0 for different angles of attack. As can be seen, a low pressure is formed on the upper surface and the region widens with increasing angle of attack up to 8°.

At higher angles, it seems that the low-pressure region still exists at the upper surface. However, the values of the low-pressure region are higher than those of the lower angle of attack. It is explained by a linear increase of lift at angles of attack below 8°, as shown in Fig. 4. The characteristics of Ishii airfoil are very different from normal airfoil, where the stall angle is around 14-16°. The unique type of pressure distribution is explained for this reason.

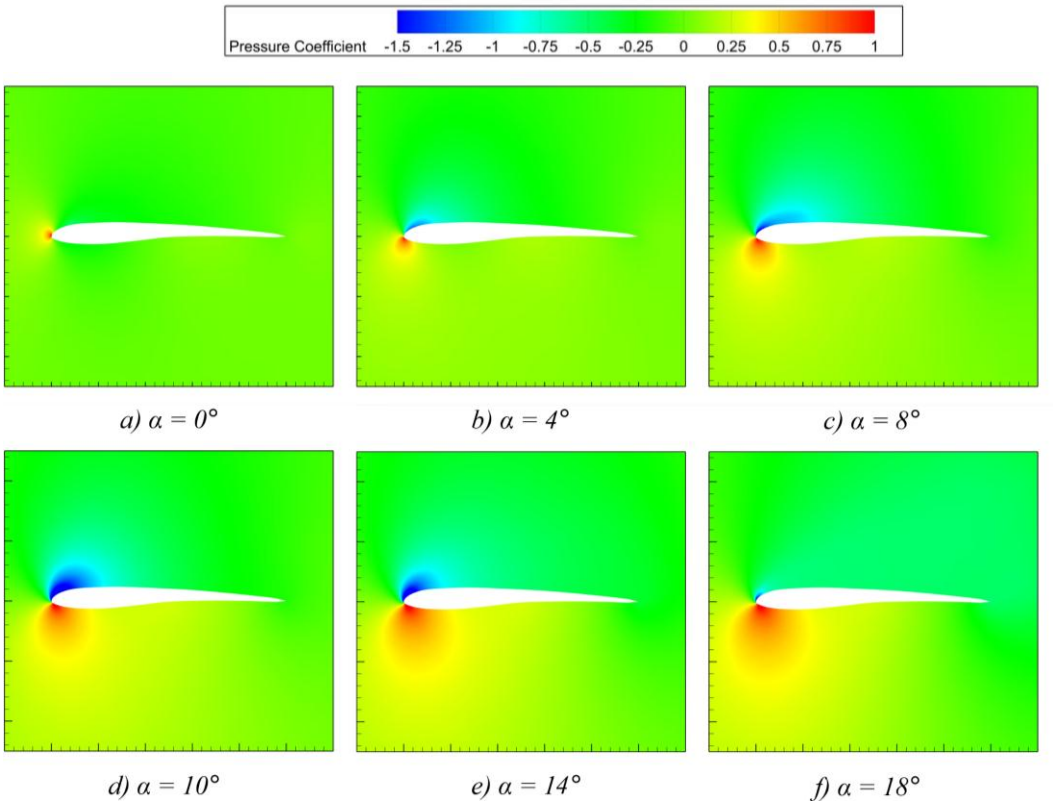

Fig. 5. Pressure distribution around airfoil at different angle of attack.

For the details of the lift trend, Fig. 6 presents the velocity magnitude in a symmetric plan mixing with streamlines of the velocity. It can be seen that the region with high velocity at the upper surface becomes wider with increasing angle of attack. Additionally, a separation bubble is formed on the surface for α = 8°. This separation bubble occurs around the leading edge of the airfoil. For higher angles of attack, the flow is fully separated on the upper surface. This separation region is significantly large at α = 18°. However, this structure is probably stable, which results in high lift as shown in Fig. 4a. Note that the current results of the streamlines are only qualitative. For details of the separation and reattachment position, other methods should be presented.

The detailed results of the separation and reattachment position will be shown in the next section.

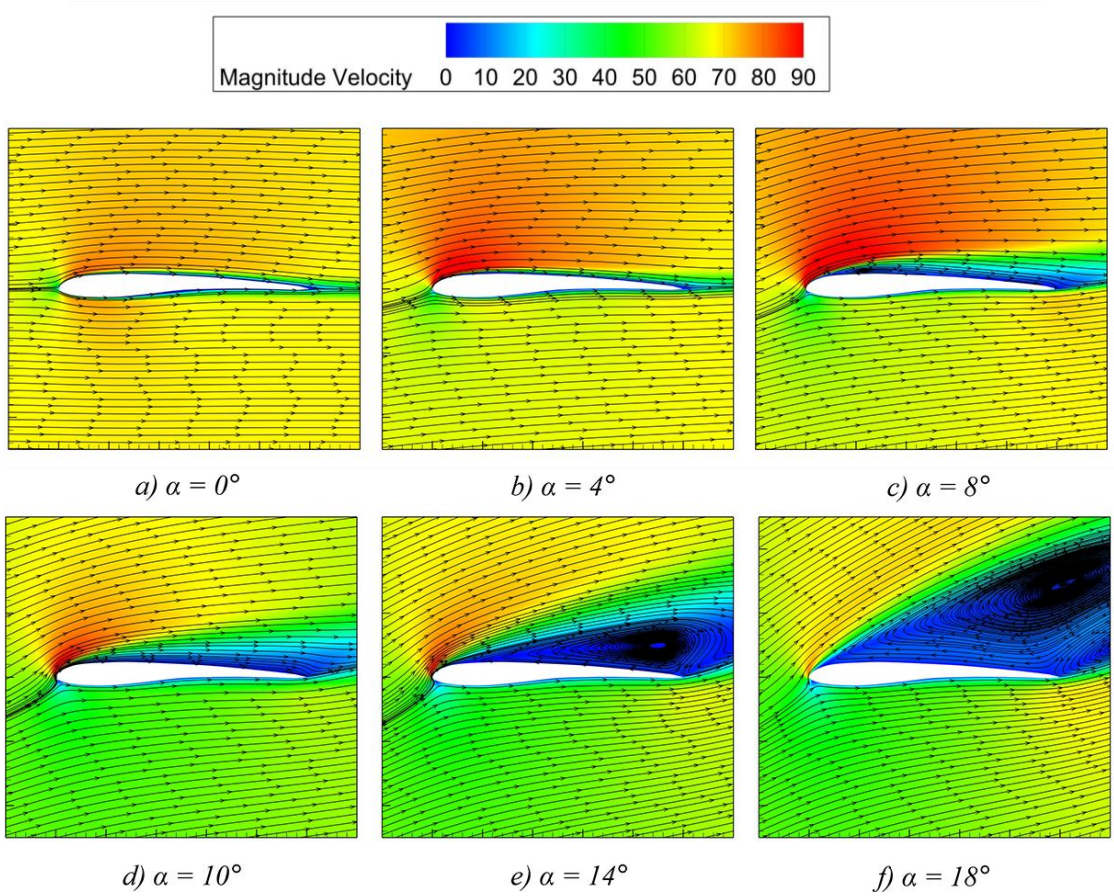

Fig. 6. Velocity and streamlines around the model at different angles of attack.

3.3. Separation and reattachment positions

For the details of the separation flow behavior, Fig. 7a shows the streamwise skin friction and Fig. 7b summarizes the separation and reattachment position on the upper surface of the airfoil at different angles of attack. Here, the separation and reattachment positions are determined from streamwise skin friction on the surface, where the skin friction changes from positive to negative for separation points and from negative to positive for reattachment points. The method was widely used previously and the location points can be obtained from the skin friction as shown in Fig. 7a. The separation and reattachment positions allow to predict the pressure distribution on the surface and therefore the lift and drag of the model. In detail, when a separation bubble occurs, the pressure distribution on the surface becomes flattened. As can be seen, the attached flow remains for the angle of attack up to 4° while the separation bubble at the

leading edge occurs for angles from 6° to 8°. At α = 6°, for example, the flow separates at around x/c = 0.08 and reattaches again at x/c = 0.3 (Fig. 7a). However, the flow attaches again on the surface at α = 10°. At a higher angle, the flow is fully on the upper surface, resulting in large aerodynamic drag. These characteristics of the Ishii airfoil are quite different from normal airfoils, where the separation bubble flow is often not generated and separation flow often occurs from the trailing edge. This kind of flow behavior results in the lift at a high angle of attack as shown in Fig. 4.

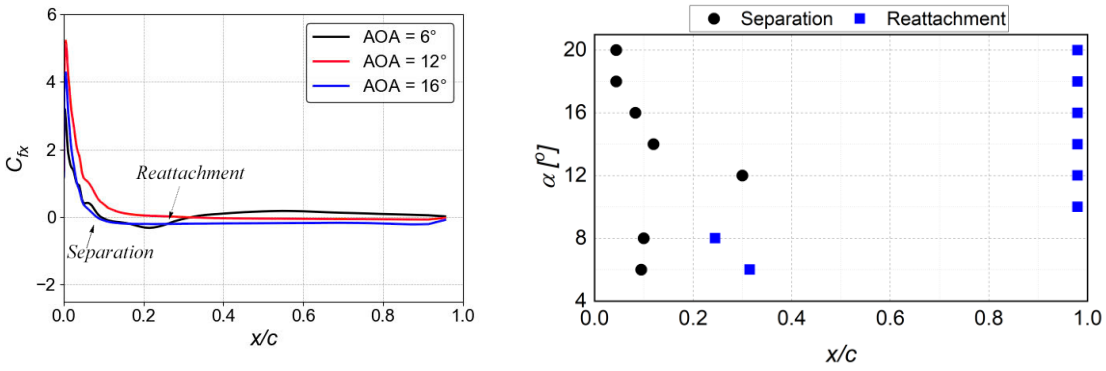

a) Streamwise skin friction *b) Separation and reattachment*

Fig. 7. Skin friction, separation, and reattachment around airfoil.

3.4. Proper Orthogonal Decomposition

In Fig. 5, it was shown that the lift of the model at angles of attack of 10° and higher at 18° is similar. However, Fig. 6 presents a high difference in wake structure. It is interesting to analyze the dynamic wake structure of the model for the different flow scenarios. In this section, the Proper Orthogonal Decomposition (POD) is applied to the simulation. The POD has gained popularity as a technique for analyzing turbulent flows, as summarized by Berkooz [16]. In this method, the fluctuation of instantaneous data fields such as velocity or pressure is treated as a snapshot ensemble. These data are organized into a matrix A, where each column represents instantaneous values of the velocity at a specific time t. The Singular Value Decomposition (SVD) of A is then performed as $A = U\Sigma V$ where Σ contains the singular values on its diagonal, and U and V represent the spatial and temporal distributions of the corresponding modes. The matrix U can be reconstructed to reveal the spatial distribution of velocity modes, while V describes the temporal evolution of the modes. A key advantage of POD analysis is that its eigenvalues prioritize the most energetic fluctuations in the input data, meaning the first modes correspond to large-scale structures, which dominate the flow fields.

For details of the technique and data processing, readers can refer to previous studies by Tran *et al.* [17] and Pham *et al.* [18].

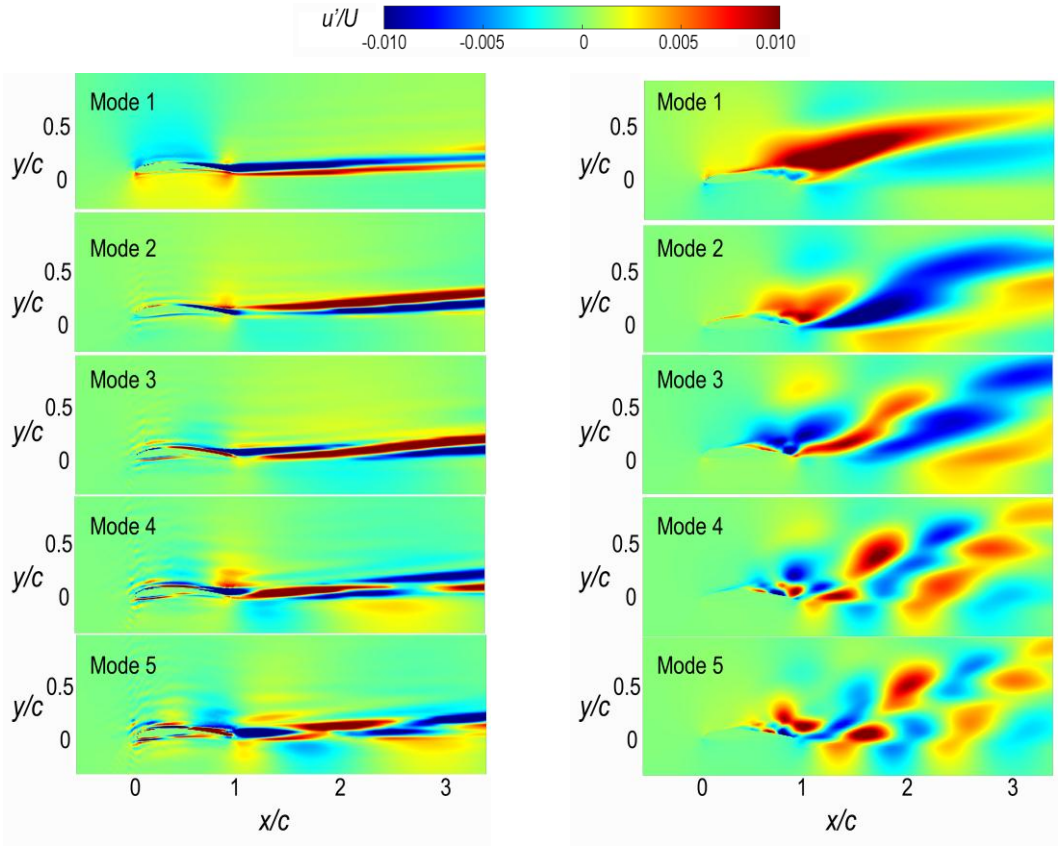

a) α =10° *b) α =18°*

Fig. 8. The first five POD modes for different angle of attack.

To generate the velocity for POD analysis, a detached eddy simulation is applied. Note that in Unsteady Reynolds-Averaged Navier-Stokes (URANS) simulations or at low angle of attack velocity fluctuations are minimal, limiting the model's ability to capture the temporal evolution of turbulent flows, as noted by Menter [15]. Consequently, this study focuses on only two typical angles of attack 10° and 18°. A Matlab program was developed for data processing. Since this study focuses only on large-scale structures, a dataset of 100 samples, taken in 0.1 s is used for analysis. Additionally, only flow on the symmetric plane is analyzed to avoid the large side vortex structure.

Figure 8 presents the first five modes of the flow for the above two angles of attack. As can be seen at α =10°, the fluctuation of the velocity is small and the flow is dominant by different symmetric modes. In detail, mode 1 and mode 2 have similar

structures but different signs. Similarly, mode 3 and mode 4 have similar structure with a half-length of mode 1 and mode 2. However, the flow is highly changed for large angles of attack with a large fluctuation. Here, the unsymmetric flow with large fluctuation occurs above the airfoil at mode 1. It is shown that the unsymmetric mode is the most dominant of the flow. The pair symmetric vortex occurs from mode 2. For the details, mode 2 and mode 3 are a pair, and mode 4 and mode 5 are a pair. The pattern of those modes indicates that modes 4 and 5 are sub-harmonic motion of the modes 2 and 3. This structure is similar to axisymmetric base flow, which was shown by Pham *et al.* [18] and by Gentile *et al.* [19]. Note that for POD analysis, further investigation of dominant frequencies and energy distribution should be conducted. However, since each POD mode contains several frequencies and this study focuses only on averaged flow with the pattern of mode, the frequencies were not analyzed. For high accuracy of the frequencies, smaller step time of the simulation and higher number of sample data should be captured.

3.5. Effect of serration at leading edge on the lift and drag behavior

Since the Ishii airfoil is designed for low Reynolds number conditions, which is similar to the working condition of the animal, it is interesting to know whether the previous design of nature can work well or not. In fact, to increase lift and reduce drag, the wings of animals such as dragonflies or birds are often designed thin with serration at the leading edge. The existence of the serration is helpful for the animal at high angles of attack, when the separation flow occurs. In this section, we investigate the effect of leading-edge configuration on the lift and drag of the model to understand its effect on the aerodynamic forces. Two leading-edge designs Modified 1 and Modified 2 and the original model are shown in Fig. 9. The selection of serration is similar to that by Mageol *et al.* [7] for flat plate in similar flow conditions. Consequently, a qualitative comparison can be made. Here, the height of serration is changed while its wide is remained. The mesh generation, numerical methods, and data processing are similar to the previous section for the original case. Note that in comparison to the original model, the modified models are little bit wider due to the existence of the peak. To calculate the lift and drag coefficients, the characteristic area is also changed.

Figure 10 presents the results of lift and drag coefficients for different angles of attack. As can be seen, when the angle of attack is small ($\alpha < 8°$), the original wing shows better lift coefficient and lower drag. The use of serration reduces lift up to 5% in comparison to the original case. However, at $\alpha > 8°$, where separation occurs on the upper surface, the serration models help to increase lift of around 4%. Additionally, the drag is also smaller, which helps to improve the aerodynamic performance of the

wing. It can be explained that the serration reduces the separation flow on the surface, resulting in an increase in lift. Since animals often fly at high angles of attack, the serration at the leading edge of the wing is an important feature, which can be observed in nature.

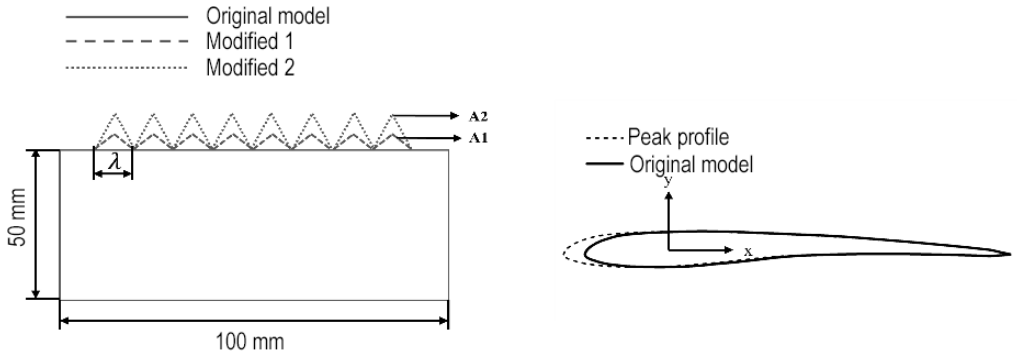

Fig. 9. Ishii wing with serration.

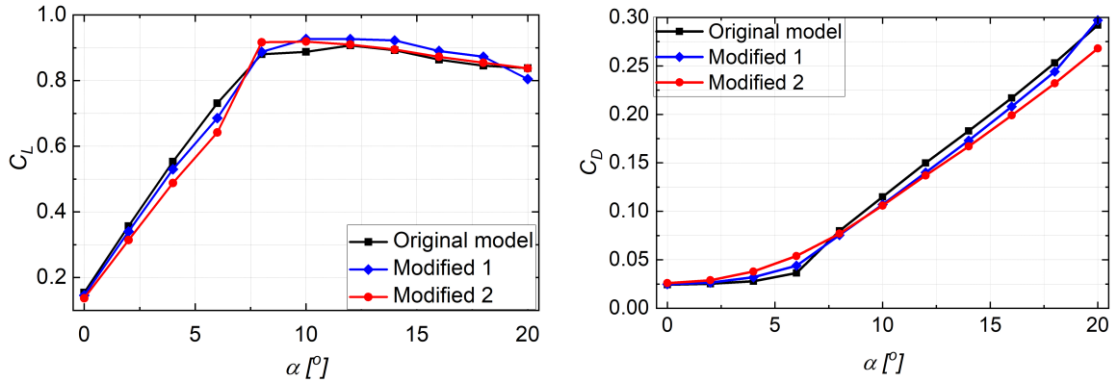

Fig. 10. Lift and drag coefficients for different configurations of the serration.

Figure 11 presents the aerodynamic performance of different serration models. As can be seen that the original model provides the highest aerodynamic performance with a maximum value of around 20. The modified models provide lower maximum aerodynamic performance. However, they are effective at high angles of attack with higher aerodynamic performance. Clearly, the serration works well when separation flow occurs on the surface. Note that the effect of serration on the aerodynamic performance of the thin airfoil was not presented in previous study. It is another important contribution of the current investigation.

Figure 12 draws the Q-criterion and the velocity in symmetric plane at 12° angle of attack for three models. The value of Q-criterion is Q = 1000. As can be seen that in

the original model, the upper surface is featured by a large velocity region, which covers the whole surface. Around the two side edges, longitudinal vortices are observed.

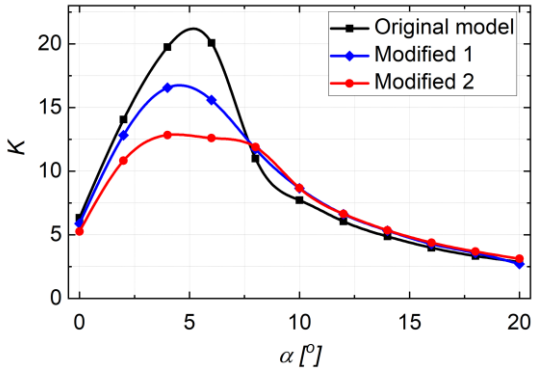

Fig. 11. Aerodynamic performance of the model with serration.

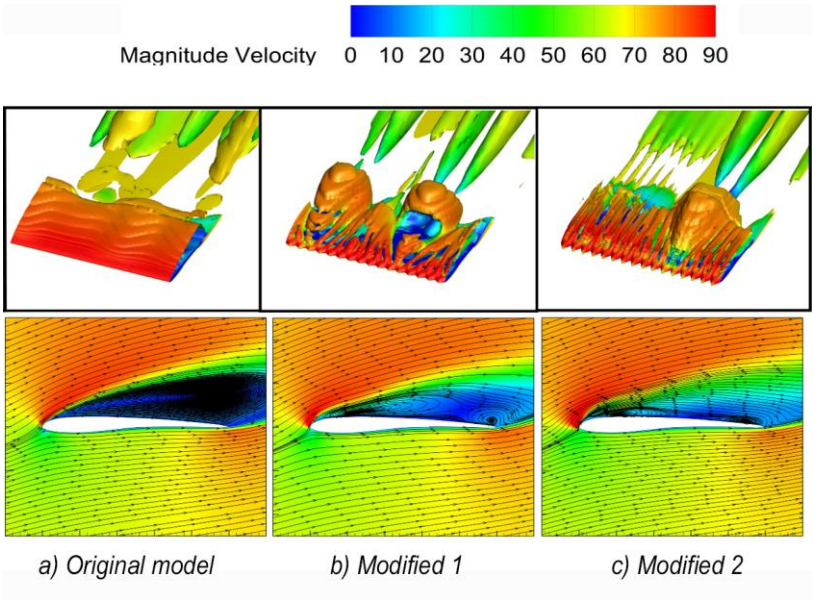

Fig. 12. Q-criterion and flow in the symmetric plane for three models.

However, when the serration is made, the large velocity structure is divided into small ones. As a result, the separation reduces and the wake structure becomes narrower. It is also explained that the lift of the model increases. It confirms that the serration is effective at high angle of attack for increasing aerodynamic performance. Our results are similar to previous observation by Mangeol *et al.* [7] for the flat plate. However, the serration on low-Reynolds number Ishii airfoil is conducted firstly in this study.

3.6. Effect of Mach number on the lift and drag behavior

Figure 13 presents the effect of the Mach number on the lift and drag coefficients for different angles of attack. Note that the compressible condition is used for different Mach number. As can be seen, the Mach number mainly affects aerodynamic force at angles of attack from 8° to 12°, where stall occurs. In detail, the stall angle and maximum lift coefficient increase with the Mach number. It can be explained by the fact that the compressible flow is highly effective in increasing the kinetic energy at the upper surface and therefore the flow attaches to the surface at a higher Mach number. Interestingly, the drag also decreases in that range of angles of attack, which helps to increase the aerodynamic performance of the model at a high Mach number.

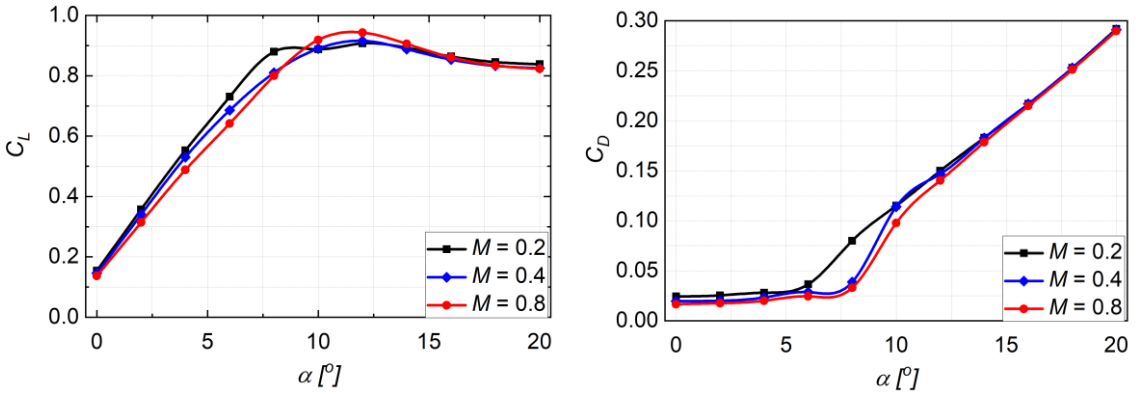

Fig. 13. Effect of Mach number on lift and drag at different angles of attack.

Figure 14 summarizes the separation and reattachment at the upper surface of the original model for different Mach number and angle of attack. The method for determining those positions was presented in Section 3.3. Note that due to the high data number, there are many steps for determining the separation and reattachment from the numerical data. However, the determination of the method is corrected and was used previously by several recent studies [20]-[22]. Some striking features should be noted for the results. Firstly, the separation bubble is also generated for M = 0.4. However, the length of the separation bubble is much smaller than that at M = 0.2. Secondly, the separation bubble disappears for M = 0.8. It is explained by the fact that the energy of the fluid becomes high at this Mach number, and flow changes into turbulent boundary condition without the transition region. Lastly, the separation positions are highly similar for α > 14° for all Mach number cases. It is also explained for the results in Fig. 13, where the lift and drag are less sensitive to Mach number at high angles of

attack. Interestingly, although the numerical scheme used in this study is low-cost and some measurement errors can occur, the striking results are presented. Additionally, it should be validated for different numerical schemes.

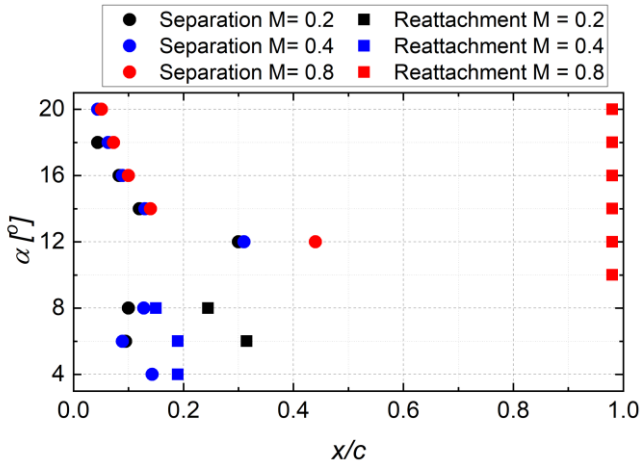

Fig. 14. Summary of separation and reattachment positions at different Mach numbers.

4. Conclusion

The effect of angle of attack, Mach number, and serration at the leading edge on the aerodynamic characteristics of Ishii airfoil was studied in this study at low Reynolds number conditions by numerical method. The main conclusion is as follows:

A highly effective model was developed for the simulation. The *k-ω* SST turbulent model is recommended to use for angles of attack below 8°, while the *k-ε* model with adjustment should be applied for higher angles of attack to get highly accurate aerodynamic results of for low-Reynolds number airfoil. The difference in the lift between previous and current studies is less than 9%, which occurs mainly at high angle of attack.

The aerodynamic characteristics of Ishii airfoil was studied extensively for different Mach numbers, and geometries of the leading edge. For the original airfoil model at M = 0.2, the angle of attack with maximum lift coefficient is around 8° and the maximum aerodynamic performance is around 4°-6°. A separation bubble was observed around the leading edge of the airfoil model at the angles of attack between 6° and 8°. Increasing the Mach number results to growth of angles of attack with maximum lift. At high angles of attack, the lift decreases but a large stall angle does not occur. These typical aerodynamic characteristics differ from normal airfoils.

The POD analysis for two typical angles of attack indicates that a symmetric pair mode occurs at a low angle of attack. However, the unsymmetric flow with a large wake structure is the most dominant flow at the high angles. The pair symmetric vortex occurs from the mode 2. Higher modes are known as sub-harmonic modes of lower.

This study first investigated the effect of serration on the aerodynamic characteristics of Ishii airfoil. The serration is helpful for angles of attack above 8° with an increasing lift of around 4%. The angle of attack with maximum lift increases with Mach number.

Although an effective simulation model was proposed, other high-accurate simulation schemes, such as detached eddy simulation and large eddy simulation, should be conducted for the model at different Mach numbers and serration conditions. The selection scheme for serration with minimum drag should be conducted. The dominant frequencies of the POD modes should be investigated. Additionally, the unsteady flow characteristics with separation is an important task for further studies.

Acknowledgment

This research is funded by Le Quy Don Technical University Research Fund under the grant number 24.1.34.

References

[1] H. Almatroushi *et al.*, "Emirates Mars mission characterization of Mars atmosphere dynamics and processes", *Space Science Reviews*, Vol. 217, No. 8, p. 89, 2021. DOI: 10.1007/s11214-021-00851-6

[2] B. Balaram *et al.*, "Mars helicopter technology demonstrator", in *2018 AIAA Atmospheric Flight Mechanics Conference*, 2018. DOI: 10.2514/6.2018-0023

[3] M. Anyoji *et al.*, "Computational and experimental analysis of a high-performance airfoil under low-Reynolds-number flow condition", *Journal of Aircraft*, Vol. 51, No. 6, pp. 1864-1872, 2014. DOI: 10.2514/1.C032553

[4] L. Caros *et al.*, "Direct numerical simulation of flow over a triangular airfoil under Martian conditions", *AIAA Journal*, Vol. 60, No. 7, pp. 3961-3972, 2022. DOI: 10.2514/1.J061454

[5] L. Caros *et al.*, "Optimization of triangular airfoils for Martian helicopters using direct numerical simulations", *AIAA Journal*, Vol. 61, No. 11, pp. 4935-4945, 2023. DOI: 10.2514/1.J063164

[6] P. Zhao *et al.*, "Review of key technologies of rotary-wing Mars UAVs for Mars exploration", *Inventions*, Vol. 8, No. 151, 2023. DOI: 10.3390/inventions8060151

[7] E. Mangeol *et al.*, "Compressibility effects on flat-plates with serrated leading-edges at a low Reynolds number", *Experiments in Fluids*, Vol. 58, pp. 1-15, 2017. DOI: 10.1007/s00348-017-2443-6

[8] T. A. Smith and C. A. Klettner, "Airfoil trailing-edge noise and drag reduction at a moderate Reynolds number using wavy geometries", *Physics of Fluids*, Vol. 34, 2022. DOI: 10.1063/5.0120124

[9] D. Miklosovic *et al.*, "Leading-edge tubercles delay stall on humpback whale (Megaptera novaeangliae) flippers", *Physics of Fluids*, Vol. 16, L39-L42, 2004. DOI: 10.1063/1.1688341

[10] F. Avallone *et al.*, "Noise reduction mechanisms of sawtooth and combed-sawtooth trailing-edge serrations", *Journal of Fluid Mechanics*, Vol. 848, pp. 560-591, 2018. DOI: 10.1017/jfm.2018.377

[11] Y. S. Hu *et al.*, "Noise reduction mechanisms for insert-type serrations of the NACA-0012 airfoil", *Journal of Fluid Mechanics*, Vol. 941, A57, 2022. DOI: 10.1017/jfm.2022.337

[12] D. J. Moreau and C. J. Doolan, "Noise-reduction mechanism of a flat-plate serrated trailing edge", *AIAA Journal*, Vol. 51, No. 10, pp. 2513-2522, 2013. DOI: 10.2514/1.J052436

[13] J. Lin *et al.*, "Shape optimization and hydrodynamic simulation of a Magnus anti-rolling device based on fully parametric modeling", *Physics of Fluids*, Vol. 35, No. 5, 2023. DOI: 10.1063/5.0152179

[14] H. T. Tran *et al.*, "Afterbody longitudinal cavities for drag reduction and application of artificial neural network for optimization of groove geometry", *Physics of Fluids*, Vol. 37, No. 3, 2025. DOI: 10.1063/5.0256556

[15] F. R. Menter, "Two-equation eddy-viscosity turbulence models for engineering applications", *AIAA Journal*, Vol. 32, No. 8, pp. 1598-1605, 1994. DOI: 10.2514/3.12149

[16] G. Berkooz *et al.*, "The proper orthogonal decomposition in the analysis of turbulent flows", *Annual Review of Fluid Mechanics*, Vol. 25, No. 1, pp. 539-575, 1993.

[17] H. T. Tran *et al.*, "Frequency characteristics of axisymmetric conical boattail models with different slant angles", *Physics of Fluids*, Vol. 35, 2023. DOI: 10.1063/5.0160053

[18] K. V. Pham *et al.*, "Delayed detached eddy simulation for wake flow analysis of axisymmetric boattail models under low-speed conditions", *Physics of Fluids*, Vol. 36, 2024. DOI: 10.1063/5.0188363

[19] V. Gentile *et al.*, "Afterbody effects on axisymmetric base flows", *AIAA Journal*, Vol. 54, No. 8, pp. 2285-2294, 2016. DOI: 10.2514/1.J054733

[20] D. Lee *et al.*, "Mechanisms of surface pressure distribution within a laminar separation bubble at different Reynolds numbers", *Physics of Fluids*, Vol. 27, 2015. DOI: 10.1063/1.4913500

[21] T. H. Tran *et al.*, "Effect of boattail angles on the flow pattern on an axisymmetric afterbody surface at low speed", *Experimental Thermal and Fluid Science*, Vol. 99, pp. 324-335, 2018. DOI: 10.1016/j.expthermflusci.2018.07.034

[22] T. H. Tran *et al.*, "Effect of boattail angle on near-wake flow and drag of axisymmetric models: A numerical approach", *Journal of Mechanical Science and Technology*, Vol. 35, No. 2, pp. 563-573. 2021. DOI: 10.1007/s12206-021-0115-1

MÔ HÌNH MÔ PHỎNG HIỆU QUẢ CAO TRONG PHÂN TÍCH KHÍ ĐỘNG CỦA CÁNH MÁY BAY Ở SỐ REYNOLDS THẤP

Trần Thế Hùng[1], Nguyễn Ngọc Thế[2], Phạm Văn Duy[3], Lê Đình Anh[2]

[1]*Khoa Hàng không Vũ trụ, Trường Đại học Kỹ thuật Lê Quý Đôn*

[2]*Viện Kỹ thuật hàng không, Trường Đại học Công nghệ, Đại học Quốc gia Hà Nội*

[3]*Trường Cơ khí, Đại học Bách khoa Hà Nội*

Tóm tắt: Gần đây, rất nhiều nghiên cứu được thực hiện cho biên dạng cánh ở điều kiện số Reynolds nhỏ và số Mach lớn nhằm cải thiện thiết kế cho dạng máy bay hoạt động trên sao Hoả và tầng bình lưu của trái đất. Trong nghiên cứu này, các đặc tính khí động của biên dạng cánh điển hình, có tên gọi là cánh Ishii, được nghiên cứu bằng phương pháp số nhằm đánh giá các lực khí động và dòng chảy trên cánh tại các góc tấn và số Mach khác nhau. Để giảm thời gian tính toán, phương pháp trung bình theo Reynolds được sử dụng cho mô phỏng. Các kết quả mô phỏng được so sánh với thực nghiệm trước đây tại cùng điều kiện dòng chảy. Nghiên cứu này chỉ ra rằng mô hình mô phỏng cần thay đổi từ k-ω SST cho góc tấn dưới 8° sang mô hình k-ε cho góc tấn lớn hơn nhằm thu được kết quả chính xác. Khác biệt lớn nhất giữa kết quả thực nghiệm và mô phỏng dưới 9%. Để mở rộng kết quả nghiên cứu, đặc tính khí động được nghiên cứu cho góc tấn từ 0° tới 20° và số Mach giữa 0,2 và 0,8. Ảnh hưởng của răng cưa tại mép trước cánh tới đặc tính khí động cũng được khảo sát. Các kết quả nghiên cứu chỉ ra rằng góc tấn với lực nâng lớn nhất khoảng 8° tại M = 0,2 và góc này tăng cùng số Mach. Tại góc tấn lớn, lực nâng của cánh giảm, nhưng hiện tượng thất tốc lớn không xảy ra. Nguyên nhân của hiện tượng này là do sự hình thành của vùng xoáy kín tại mép trước của cánh, điều này khác biệt so với mô hình cánh máy bay thông thường. Cánh với răng cưa ở mép trước giúp tăng lực nâng và chất lượng khí động cho góc tấn trên 8°. Kết quả của phép trực giao riêng phân chỉ ra rằng cấu trúc dòng chảy bất đối xứng với vùng xoáy lớn là cấu trúc đặc trưng của dòng chảy tại góc tấn lớn. Hình ảnh dòng chảy của các chế độ khí động, phân bố vận tốc, áp suất quanh mô hình được thảo luận.

Từ khóa: *Biên dạng cánh Ishii; động lực học tính toán; máy bay sao Hỏa; số Mach; góc tấn.*

Received: 07/02/2025; Revised: 30/03/2025; Accepted for publication: 23/05/2025

❑